RESEARCH ARTICLE

Key Points:
- Analytic solution of toroidal oscillations in finitely conducting ionosphere
- Behavior of Alfven mode in different limits of Pedersen conductance
- Analytic estimates of mode frequency and damping coefficient

Correspondence to:
J. Bulusu,
bulusujayashree@gmail.com

Role of finite ionospheric conductivity on toroidal field line oscillations in the Earth's magnetosphere — Analytic Solutions

Jayashree Bulusu[1,2], A. K. Sinha[1], and Geeta Vichare[1]

[1]Indian Institute of Geomagnetism, Mumbai, India, [2]Now at National Geophysical Research Institute, Hyderabad, India

Abstract An analytic solution has been formulated to study the role of ionospheric conductivity on toroidal field line oscillations in the Earth's magnetosphere. The effect of ionospheric conductivity is addressed in two limits, viz, (a) when conductance of Alfvén wave is much different from ionospheric Pedersen conductance and (b) when conductance of Alfvén wave is close to the ionospheric Pedersen conductance. In the former case, the damping is not significant and standing wave structures are formed. However, in the latter case, the damping is significant leading to mode translation. Conventionally, "rigid-end" and "free-end" cases refer to eigenstructures for infinitely large and vanishingly small limit of ionospheric conductivity, respectively. The present work shows that when the Pedersen conductance overshoots (undershoots) the Alfvén wave conductance, a free-end (rigid-end) mode gets transformed to rigid-end (free-end) mode with an increase (decrease) in harmonic number. This transformation takes place within a small interval of ionospheric Pedersen conductance around Alfvén wave conductance, beyond which the effect of conductivity on eigenstructures of field line oscillations is small. This regime of conductivity limit (the difference between upper and lower limits of the interval) decreases with increase in harmonic number. Present paper evaluates the damping effect for density index other than the standard density index $m = 6$, using perturbation technique. It is found that for a small departure from $m = 6$, both mode frequency and damping rate become a function of Pedersen conductivity.

1. Introduction

In magnetospheric research, profound importance is given to understand the magnetosphere-ionosphere coupled system. Geomagnetic pulsations, observed on ground and space, are one of the many signatures that are the result of this coupled system. It was first proposed by *Dungey* [1954] that these pulsations are the consequences of standing Alfvén oscillations on discrete field lines. Many earlier researchers have brought insights to the nature of these oscillations in background cold magnetosphere using magnetohydrodynamic approach [*Radoski*, 1967; *Cummings et al.*, 1969; *McClay*, 1970; *Orr and Mathew*, 1971; *Southwood*, 1974; *Hughes*, 1974; *Newton et al.*, 1978; *Singer et al.*, 1981]. The cold plasma waves (Shear Alfvén mode and compressional mode) are theoretically decoupled to toroidal and poloidal modes depending on whether the perturbed magnetic field is contained in the azimuthal or meridional directions, respectively [*Orr*, 1973]. There have been many theoretical as well as observational studies of toroidal and poloidal modes in the past [*Cummings et al.*, 1969; *Engebretson et al.*, 1986; *Anderson et al.*, 1990; *Sinha et al.*, 2005; *Bochev and Sinha*, 2010; *Liu et al.*, 2013; *Takahashi et al.*, 2013]. There are many other discrete oscillations observed in the inner magnetosphere of the Earth. *Agapitov et al.* [2008] investigated the generation of ballooning modes in the inner magnetosphere of the Earth in the dipole model of the geomagnetic field. They considered the ionosphere as a thin layer with finite conductivity and reported discrete eigenmode structures that consist of Alfvén, slow magnetosonic, flute, and incompressible modes. It was demonstrated that the interaction between these modes depended on ionospheric conductivity.

It is important to note that the basic formation of these standing structures is due to the reflection at the ionosphere. One of the widespread assumption is that the ionosphere has significant conductivity to reflect the incident Alfvén waves completely. Under this assumption, the geomagnetic field lines are fixed to the ionosphere at the conjugate points, forming the fixed/rigid-end mode [*Cummings et al.*, 1969; *Sinha and Rajaram*, 1997]. In this mode, the incident electric field is completely reflected. However, the magnetic field has a finite component at the ionosphere. On the other hand, when the ionospheric conductivity is vanishingly small,

the magnetic field associated with Alfvén mode is completely reflected and new set of standing waves are generated. This is termed as the free-end mode [*Newton et al.*, 1978; *Allan and Knox*, 1979a]. The associated electric field has a finite component in the ionosphere. Rigid-end and free-end modes are formed when conjugate ionospheres are symmetric. Rigid-end and free-end modes are special cases of half wave mode. There exists another case where one of the ionospheres have very high conductivity in contrast to the other conjugate point, leading to formation of quarter wave modes whose periods are twice that of half waves [*Allan and Knox*, 1979a, 1979b; *Budnik et al.*, 1998; *Obana et al.*, 2008; *Bulusu et al.*, 2014a].

A comprehensive analytic model discussing the rigid-end, free-end, and quarter wave toroidal modes is presented in our earlier papers [*Sinha and Rajaram*, 1997; *Bulusu et al.*, 2014a, 2015b]. The main focus of our study was development of a theoretical model that can explain different types of standing Alfvén oscillations in different regimes of ionospheric conductivity. The reflection at the ionosphere is decided by the balance between the height integrated Pedersen conductance and conductance of Alfvén wave at the conjugate point. The reflection coefficient at the ionosphere can be computed using the relation given by *Scholer* [1970] as $R = \frac{\Sigma_P^{N,S} - \Sigma_A}{\Sigma_P^{N,S} + \Sigma_A}$. Σ_P denotes the height-integrated conductivity, and superscripts N and S represent the northern and southern conjugate, respectively. For the Alfvén speed V_A along the field line, the wave conductance (Σ_A) is defined as $\Sigma_A = \frac{1}{\mu_0 V_A}$ [*Scholer*, 1970]. For half waves, either $\Sigma_P^{N,S} \ll \Sigma_A (R = -1)$ or $\Sigma_P^{N,S} \gg \Sigma_A (R = +1)$ holds good. These modes are formed when the ionospheres have infinitely large or infinitesimally small symmetric conductivity at the conjugate ionospheres. These are ideal cases and are discussed in our earlier study [*Sinha and Rajaram*, 1997; *Bulusu et al.*, 2014a]. However, for quarter waves, either $\Sigma_P^N \ll \Sigma_A (R = -1)$ in northern conjugate point and $\Sigma_P^S \gg \Sigma_A (R = +1)$ in southern conjugate point or $\Sigma_P^N \gg \Sigma_A (R = +1)$ in northern conjugate point and $\Sigma_P^S \ll \Sigma_A (R = -1)$ in southern conjugate point are satisfied. These modes are most likely observed during June and December solstices [*Allan and Knox*, 1979a; *Budnik et al.*, 1998; *Obana et al.*, 2008; *Bulusu et al.*, 2015a]. A detailed theoretical computation of quarter wave toroidal wave was discussed by *Bulusu et al.* [2014a]. They formulated the field-aligned structures of electric and magnetic field associated with quarter wave. They also established the relation between half and quarter wave toroidal oscillations.

However, the situation of real ionosphere is rather complicated. The existence of finite conductivity in the ionosphere simultaneously reflects and absorbs the incident Alfvén wave. The effect is twofold. First, the 90° rotation of the transverse magnetic field perturbation by ionospheric Hall effect is significant in relation to geomagnetic pulsations in the high-latitude regions [*Dungey*, 1963; *Nishida*, 1964; *Tamao*, 1964; *Inoue*, 1973; *Hughes*, 1974; *Hughes and Southwood*, 1976]. Second, the ionosphere is regarded as the Joule dissipation region for the modes of field line oscillations [*Newton et al.*, 1978; *Allan and Knox*, 1979a, 1979b; *Yoshikawa et al.*, 1999; *Southwood and Kivelson*, 2000, 2001]. *Inoue* [1973], *Hughes* [1974], and *Hughes and Southwood* [1976] have given detailed analysis of the effect of the atmosphere and ionosphere on incoming traveling wave fields. They showed that under the assumption of thin sheet ionosphere, the signature of magnetic field associated with the incoming traveling wave is mapped to the ionosphere through the Pedersen conductivity. The electric field, on the other hand, is brought to ground through the Hall conductivity. However, in their study they considered a plane geometry implying an infinite flat Earth; and hence, realistic geometrical restrictions on the wave were not included.

Many researchers have provided the numerical solutions to the eigenmode structure in finite ionospheric conductivity [*Newton et al.*, 1978; *Streltsov and Lotko*, 1996; *Yoshikawa and Itonaga*, 1996; *Yoshikawa et al.*, 1999; *Yagova et al.*, 1999; *Nakata et al.*, 2000; *Ozeke and Mann*, 2005; *Lysak*, 2004] in different ambient field geometries. *Newton et al.* [1978] showed that magnetospheric signals get shielded by Pedersen currents flowing in the ionosphere. They attributed the effect of finite ionospheric conductivity to the wave damping at the conjugate points due to Joule heating in the ionosphere. In addition, they numerically addressed the conversion of mode from rigid end to free end and vice versa in different conductivity limits. The formation or transformation of standing Alfvén modes is dependent on height-integrated Pedersen conductance (Σ_P), the damping rate (γ/ω_r, where γ damping associated with wave mode and ω_r the mode frequency of the wave), and the conductance of Alfvén wave (Σ_A). *Newton et al.* [1978] showed that at a fixed L shell, $\gamma/\omega_r = (2 \times 10^9) L^{3/2} / \Sigma_P$ for large Σ_P, and $\gamma/\omega_r = (2 \times 10^{-11}) \Sigma_P / L^{3/2}$ for small Σ_P. Thus, damping is small for large as well as small values of Σ_P. The rate of damping is large in the region where Σ_P is comparable to wave conductance of Alfvén wave Σ_A (i.e., $\Sigma_P \sim \Sigma_A$).

Yoshikawa and Itonaga [1996] and *Yoshikawa et al.* [1999] used numerical methods and worked in the simplified Cartesian geometry to show that there exist two cutoffs (upper and lower) of the height-integrated

Pedersen conductivity during transformation of Alfvén modes. Below the lower cutoff the ionosphere behaves like an insulator, and above the upper cutoff the ionosphere behaves like a perfect conductor. In between these two limits, there exists a transition region in which the nth harmonic of insulator-like ionosphere is connected continuously to the $(n + 1)^{th}$ harmonic of Alfvén wave of the conductor-like ionosphere.

Southwood and Kivelson [2001] used the Wentzel-Kramers-Brillouin (WKB) approximation to discuss the ionospheric contribution to damping and the phase variations using a density distribution of $1/r^6$ along the field line. *Nakata et al.* [2000] numerically solved the mode equation in straight ambient field inclined to the ionosphere in the trapezoid model to bring out the dependence of magnetic perturbations on the Pedersen and Hall conductivity in the ionosphere. In their simulation, they found that the fundamental toroidal oscillations are governed by Pedersen conductivity, whereas higher harmonics are governed by Hall conductivity. However, no convincing analytic solution has been developed so far incorporating the finite ionospheric conductivity with generalized density variation.

Lysak [2004] dealt with numerical modeling of magnetosphere-ionosphere coupling by Alfvén waves using inductive approach. He found that when an incident shear Alfvén wave carrying a potential electric field is reflected from the nonisotropically conducting ionosphere, the reflected wave consists of both shear and fast mode waves. Though this approach of numerical modeling addressed the problem of magnetosphere-ionosphere coupling via Alfvén wave, the investigation did not reveal how the standing Alfvén wave could change its characteristics when Pedersen conductance was in the vicinity of Alfvén conductance.

Tu et al. [2014] numerically solved the time-dependent continuity, momentum, and energy equations for ions and neutrals, together with Maxwell's equations (Ampere's and Faraday's laws) to investigate the magnetosphere-ionosphere/thermosphere coupling via MHD waves. They addressed the coupling of magnetosphere and ionosphere during transient events and in response to an enhanced magnetospheric convection. Through their numerical simulation they could explain the overshoots and oscillations observed during substorms. They could show that the ionosphere/thermosphere behaves as a damped oscillator during substorm. The numerical work of *Tu et al.* [2014] is more relevant to enhanced magnetospheric convection during substorms.

There have been both satellite and ground observations of mode transformations between day and night terminators [*Budnik et al.*, 1998; *Obana et al.*, 2008; *Bulusu et al.*, 2015a]. These studies dealt with observation of standing wave modes using ground and satellite magnetometer data. The main focus of these studies was identification of a typical type of standing Alfvén mode (quarter waves) which is formed when the ionospheric conductivity at both ends of the field line is highly asymmetric. *Budnik et al.* [1998] and *Bulusu et al.* [2015a] carried out this study using magnetometer data from GOES satellite (altitude range $L = 6.6R_E$, where R_E is the Earth's radius). *Obana et al.* [2008] used ground magnetometer data to investigate these waves. All these studies report a considerable change of mode frequency with change in ionospheric conductivity. These mode transformations were addressed in the light of ionospheric conductivity. However, the estimate of losses accompanied during the mode transformation was not addressed. The present study would address this significant aspect and provide a tool to account for these losses. The second contribution would be identification of conductivity regimes within which the mode transformation takes place. This would also provide an indirect tool to identify the harmonic of the wave from actual observation.

In this paper, we extend analytic model developed by us to account for the effect of finite ionospheric conductivity. All the assumptions for rigid-end, free-end, and quarter wave solutions in earlier papers hold good even in the context of finite ionospheric conductivity. In section 2, we present in brief the outline of our analytic model. In sections 3 and 4, we discuss the limits of ionospheric conductance, indicating effects of different levels of damping, on standing structures of toroidal oscillations. Using present analytic model, section 4 evaluates the damping rate for density index other than the standard $m = 6$ index, using perturbation technique. We conclude our findings in section 5.

2. Direct Analytic Model (DAM)

The model is based on cold plasma approximation (plasma pressure is much less than the magnetic pressure) where plasma is treated as a fluid, and the dynamics are controlled by magnetic field. Under this condition, the magnetohydrodynamic (MHD) approach is valid and the concept of frozen-in flux holds for obtaining the

field line structures of electric and magnetic field fluctuations associated with Alfvén waves. The basic mode equation in generalized magnetic field geometry is given by the second-order mode equation by *Singer et al.* [1981]. This mode equation was derived for the low-frequency transverse waves in an infinitely conducting, stationary magnetized plasma with negligible plasma pressure and can be written as

$$\mu_o \rho \frac{\partial^2}{\partial t^2}\left(\frac{\xi_\alpha}{h_\alpha}\right) - \frac{1}{h_\alpha^2}\vec{B_o}\cdot\vec{\nabla}\left[h_\alpha^2\vec{B_o}\cdot\vec{\nabla}\left(\frac{\xi_\alpha}{h_\alpha}\right)\right] = 0 \tag{1}$$

where μ_o is the magnetic permeability in vacuum, ρ is plasma mass density, ξ_α is the plasma displacement perpendicular to the field line, and $\vec{B_o}$ is the ambient magnetic field. The parameter α determines the mode of oscillation and signifies the direction of plasma displacement. h_α is the scale factor for the normal separation between the field lines in the direction of α and is determined by the magnetic field geometry. The significance of this equation is that it is applicable to a generalized magnetic field geometry and can be solved for both toroidal and poloidal modes of field line oscillations. The complete derivation with the involved assumptions is discussed in Appendix A.

We used this mode equation to develop a single generalized solution applicable for toroidal rigid-end [*Sinha and Rajaram*, 1997], free-end [*Bulusu et al.*, 2015b], and quarter wave modes [*Bulusu et al.*, 2014a] (refer Appendix B for the complete solution). It is interesting to note that the solution of the above mode equation is valid even in the case of finite ionospheric conductivity. The solution of this mode equation which denotes the normalized displacement of toroidal oscillation at any point on the geomagnetic field lines is given by (cf. Appendix B for stepwise development of the solution).

$$X = \sqrt{\frac{1}{2L\nu}}\sqrt{\frac{V_{Aeq}}{\omega L R_E}}\frac{\eta^{1/2}}{\sin^{3-m/2}\theta}\left[J_\nu(\eta) + KJ_{-\nu}(\eta)\right] \tag{2}$$

The parameter X denotes the normalized displacement, R_E is the Earth's radius, V_{Aeq} is the Alfvén speed at the equator, ω is the mode frequency, and θ is the colatitude. $L = 1/\sin^2\theta_c$ is the geocentric distance (in R_E) of the point where the field line crosses the equator. The suffix c indicates the value at the conjugate point. $\eta = \frac{\omega L R_E}{V_{Aeq}}\int_0^\theta \sin^{7-m}\theta$ and $\nu = 1/(8-m)$, where m denotes the density index that describes the plasma distribution along the field in the form of the power law $\rho = \rho_o(r_o/r)^m$. ρ_o being the proton mass density at r_o, the geocentric distance to equatorial crossing point of the field line considered, and r is the geocentric distance to the position of interest on the field line. We also assume that the plasma consists only of protons. The arbitrary constant K plays a crucial role in this equation as it incorporates different boundary conditions at the ionosphere for rigid-end and free-end modes. K is estimated by making the solution X zero for rigid end or its derivative dX/dS zero for free end at the conjugate points [*Bulusu et al.*, 2015b]. This unique model that accounts for extreme ionospheric conductivity condition is termed as Direct Analytic Model (DAM).

Though it is theoretically cumbersome to incorporate the finite ionospheric conductivity, we have made an attempt in this direction using DAM. In order to use this solution for finite ionosphere, we assume the thin sheet ionosphere where we can assume

$$\vec{\nabla}\times\vec{b} = \mu_0\vec{j} \tag{3}$$

where $\vec{j}$ is current density, $\vec{b}$ is perturbed magnetic induction, and we have neglected displacement currents. *Baker and Martyn* [1953] have given the expression for the meridional current $\vec{j}$ as

$$j_\nu = \sigma_P E_\nu + \sigma_H E_\phi \tag{4}$$

Here j_ν represents the meridional current in the ionosphere. E_ν and E_ϕ represent the meridional and azimuthal electric fields, respectively. σ_P and σ_H denote the Pedersen and Hall conductivities, respectively. An initial E_ν, (i.e., a toroidal mode electric field) generates an E_ϕ in the ionosphere through the Hall conductance σ_H. The Pedersen conductance reflects the incident wave magnetic field, and the Hall conductance transmits the ULF signal to ground [*Hughes and Southwood*, 1976]. An isolated toroidal mode is only possible if $\sigma_H = 0$. If $\sigma_H \neq 0$, there would be an associated evanescent fast mode (or poloidal mode) [*Allan and Knox*, 1979a]. In the present work we only deal with isolated toroidal mode. Hence, we neglect the contribution from Hall conductance.

We only discuss the ionospheric reflection and neglect the atmospheric propagation, thereby neglecting the effect of Hall conductance. An inclusion of finite conductivity at the foot of the field line modifies the eigenstructure to a great extent. Also, it will lead to the flow of Pedersen current at conjugate ionospheres, and the wave energy will be lost via Joule heating [*Southwood*, 1974]. The shielding of magnetospheric signal by Pedersen currents results in the following relation at the foot of the field line in the ionosphere [*Hughes*, 1974]

$$b = \pm\mu_o \Sigma_P E \tag{5}$$

where "+" corresponds to Southern Hemisphere and "−" corresponds to Northern Hemisphere. Σ_P is the height-integrated Pedersen conductivity. The effect of finite ionospheric conductivity is embedded in the arbitrary constant K of the normal mode solution prescribed by equation (2). K in equation (2) is evaluated by using the boundary condition (equation (5)) at the conjugate point.

The perturbed magnetic field b and electric field E in the finite ionosphere can be, respectively, written as $b = h_\alpha B_0 \frac{dX}{dS}$ and $E = -i\Omega V_{Aeq} h_\alpha B_0$ (refer equations (B8) and (B9) in Appendix B for the derivation). In terms of normalized displacement X and its derivative $\frac{dX}{dS}$, equation (5) can be re written as

$$\frac{dX}{dS} \pm i\mu_o \Sigma_P \Omega V_{Aeq} X = 0 \tag{6}$$

where Ω is the normalized frequency given by $\Omega = \frac{\omega}{R_E V_{Aeq}}$. As the finite ionospheric conductivity leads to wave damping at the ionosphere due to ionospheric Joule heating, we consider the complex wave frequency $\omega = \omega_r + i\gamma$ (where $\gamma > 0 \implies$ wave damping and $\gamma < 0 \implies$ wave growth).

Ellis and Southwood [1983] have shown that there lies a regime of conductivity within which the wave is damped completely and standing wave is not possible. As mentioned earlier, the reflection coefficient at the conjugate point plays a crucial role in deciding the existence of standing mode on field lines. When $\Sigma_P^{N,S} \ll \Sigma_A$, or $\Sigma_P^{N,S} \gg \Sigma_A$, standing modes are formed. However, when $\Sigma_P^{N,S} \sim \Sigma_A$, the standing mode is not possible and mode transformation takes place. The range of conductivity within which the mode transformation takes place is defined as the critical conductivity regime. However, away from this region, it is possible to get standing Alfvén waves because of multiple reflections from ionospheres in opposite hemispheres. The deviation from this condition of ionospheric conductivity causes damping of such standing waves with damping constant

$$\gamma = \frac{V_A}{2a} \ln \frac{1}{|R|} \tag{7}$$

where $2a$ is the length of flux tube and R is the reflection coefficient. $\Sigma_A = \frac{1}{\mu_0 V_A}$ represents the conductance of Alfvén wave [*Maltsev et al.*, 1977]. In extreme limits of $\Sigma_P \ll \Sigma_A$ or $\Sigma_P \gg \Sigma_A$, $|R|=1$, and the wave is completely reflected at the conjugate point in the ionosphere. Infinite damping will occur when $R = 0$, that is, when $\Sigma_P = \Sigma_A$, and in this case no standing waves will be set up [*Newton et al.*, 1978]. It should be noted that *Ellis and Southwood* [1983] gave the estimate of γ in the box geometry of ambient magnetic field (equation (7)) and is defined particularly only for $1/r^6$ type density variation along the field line. An identical relation was developed by *Allan and Knox* [1979a] for background dipole magnetic field geometry. However, no convincing analytic estimate for mode frequency and damping has been developed so far in a generalized density variation along the field line. In the next section, we attempt to account for mode frequency and damping rate under the condition of finite conductivity at the conjugate ionosphere and discuss their implications in the limits $|R| = 1$, and $R = 0$ corresponding to $\gamma/\omega_r \ll 1$ or $\gamma/\omega_r \gg 1$, respectively. It should be noted that the damping is not important for $|R| = 1$.

3. Nature of Standing Alfvén Waves in the Vicinity of $|R| = 1$ (Negligible Damping)

In this section, we discuss the situation when the conductivities are comparable at the two conjugate points (damping is minimum). It is not any conjecture that damping was small due to a certain conductivity condition. At a conjugate point, damping is decided by the relative magnitude of height integrated Pedersen conductance and Alfvén wave conductance. It is the reflection coefficient (R) that decides the balance between these two conductivities. The damping rate γ/ω_r varies as log $(1/R)$. Hence, when $\Sigma_P^{N,S} \ll \Sigma_A$, or $\Sigma_P^{N,S} \gg \Sigma_A$, γ/ω_r would be negligible simultaneously in both Northern and Southern Hemispheres.
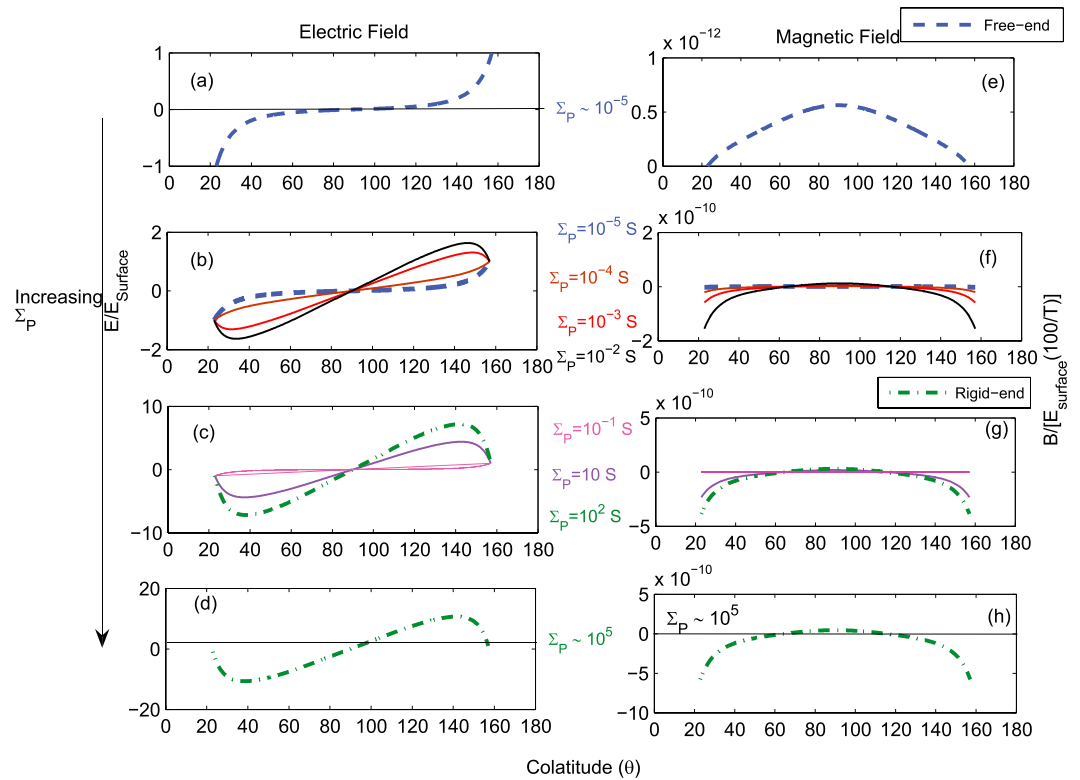
Figure 1. Latitudinal structures of electric and magnetic field with increasing Σ_P for $L = 6.6$ and $m = 5$. (a and e) Fundamental free-end electric and magnetic field for negligibly small Σ_P. (b and f) The departure of electric and magnetic field for small increase in Σ_P. (c and g) Generation of second harmonic of rigid end with a significant increase in Σ_P. (d and h) The second harmonic rigid-end electric and magnetic field structure at large values of Σ_P. The magnitude of electric field or magnetic field at any point can be obtained by multiplying with the indicated factor. $E_{surface}$ and T, respectively, represent the surface value of electric field and time period.

Even when the ratio of the conductivities between the Northern and Southern Hemisphere is around 2, the damping is still very small. The observation of continuous pulsations at geostationary height is one of the examples for this case [*Denton et al.*, 2004; *Takahashi and Denton*, 2007; *Bulusu et al.*, 2015a]. The fact that harmonics as large as 6 could be observed during day time at geostationary height suggests that a very small damping is associated with the Alfvén wave during this period [*Takahashi and Denton*, 2007].

In the extreme limits of height-integrated ionospheric Pedersen conductance Σ_P, two standing wave structures, viz, rigid end ($\Sigma_P \gg \Sigma_A$) and free end ($\Sigma_P \ll \Sigma_A$) are possible for which $R = 1$. Under these conditions $\gamma/\omega_r \ll 1$ and the mode can be characterized by the real part of frequency ω_r only, and the contribution from γ/ω_r is completely neglected. In such a case, the eigenfrequency ω_r and the field line structure can be obtained in the similar way as was obtained in case of rigid end, free end, and quarter wave by including the appropriate boundary conditions at the conjugate point and at the equator. The condition at the conjugate point is governed by equation (6), while the condition at the equator is decided by the harmonic number. In the limit $\Sigma_P \ll \Sigma_A$ (free end), at the equator $X = 0$ for odd harmonics and its derivative $\frac{dX}{dS} = 0$ for even harmonics. In order to account for spatial and temporal characteristics of toroidal oscillations, the ionospheric Pedersen conductance $\Sigma_P^{N,S}$ is considered identical, small and finite at both the conjugate points in Northern (superscript N) and Southern (superscript S) Hemispheres. As Σ_P is changed simultaneously by equal amounts at both hemispheres, it is seen that the mode changes from free end to higher harmonic rigid end.

Figure 1 depicts the transformation of the fundamental electric and magnetic field of free end to the second harmonic rigid end with increasing value of height-integrated Pedersen conductivity for a typical density index $m = 5$ at $L = 6.6$. The left-hand side of Figure 1 depicts field line structure of electric field, and the right-hand side shows the same for magnetic field. The fundamental electric and magnetic field structures for the free end are presented in Figures 1a and 1e, respectively, when the ionospheric conductivity is very small ($\sim 10^{-5}$ S). It is seen that for gradual increase in Σ_p the free-end electric field and magnetic field get modified
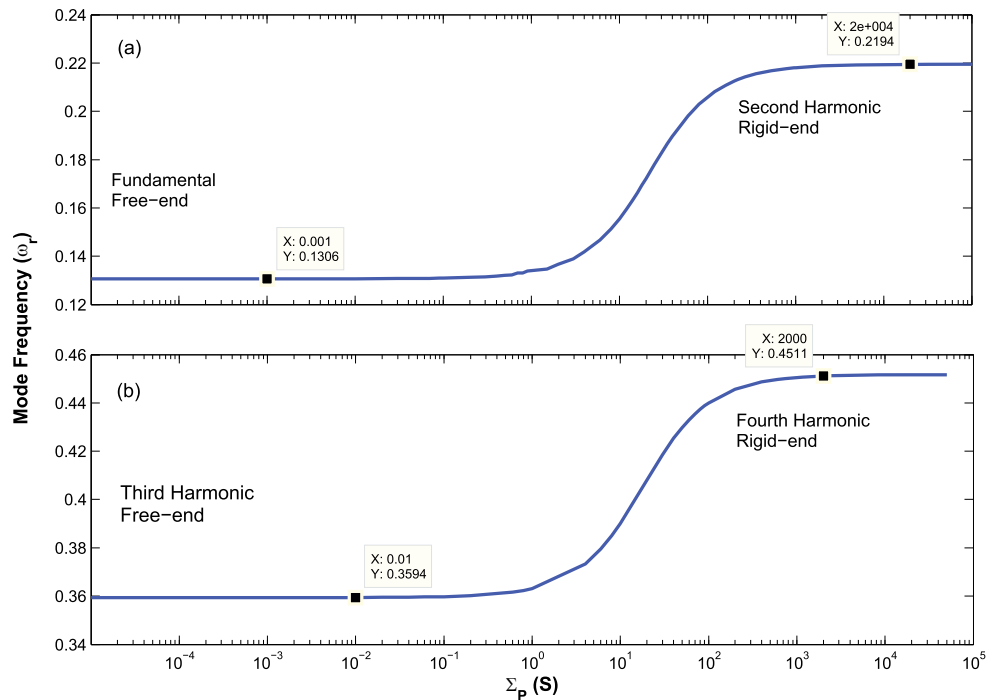
Figure 2. Frequency characteristics of free end with gradual increase in Σ_P for (a) fundamental and (b) the third harmonic.

(Figures 1b and 1f). However, the free-end structures are preserved (thick dotted blue line shown in Figures 1b and 1f) till the ionospheric conductivity is increased beyond a critical value, called the critical conductivity. The different plots correspond to different values of height-integrated conductivity (values presented in the same color). The subsequent plots in Figures 1c and 1g show that with significant increase in conductivity the antinodes of electric field tend to form nodes at the conjugate ionospheres, preserving the node at the equator. Also, a shift in the nodes from conjugate points to either side of the equator is observed in the magnetic field structure. The thick dotted green line in these figures marks the generation of the second harmonic. At very large values of Σ_P, the mode reflects the second harmonic rigid-end characteristics (Figures 1d and 1h).

From our earlier investigations we have been able to estimate the eigenfrequencies of toroidal mode under rigid-end and free-end conditions [*Sinha and Rajaram*, 1997; *Bulusu et al.*, 2015b]. In our model, we considered a proton density of 1 cm^{-3} at geosynchronous height which resulted in the wave-mode frequency 0.219 cycles/s for second harmonic of rigid end and 0.1306 cycles/s for fundamental free end of toroidal oscillation at $L = 6.6$. It is interesting to note that from the present analysis we obtain the fundamental frequency of free end, which is 0.1306 cycles/s approaches to second harmonic of rigid end 0.219 cycles/s with the gradual increase in conductivity value (Figure 2a). Also, the effect of conductivity over frequency is significant within a conductivity range, referred as critical conductivity (which is 0.003 – 1 × 10^4 S in the present case). Between these two values of critical conductivity, a small change in conductivity can lead to a steep increase in frequency. Below the lower limit of this regime, the ionosphere behaves as an insulator. Beyond the upper limit, the frequency change is again very small, and the ionosphere can be considered as a perfect conductor. The values of the critical conductivities and the order of frequency change between these two extreme limits reported here are consistent with those obtained by *Newton et al.* [1978] and *Yoshikawa et al.* [1999].

Figure 2b shows another example of the frequency conversion from third harmonic free end to fourth harmonic rigid end (corresponding field line structures of electric and magnetic field are shown in Figure 3). It can be seen that the critical conductivity regime reduces to (0.01 – 2 × 10^3 S) compared to the earlier case (0.001 – 2 × 10^{4}S). Figures 3a and 3e show that for very small conductivity ($\sim$10^{-5} S), the electric and magnetic field structures resemble the third harmonic free end. However, as Σ_P is increased the mode gradually approaches to fourth harmonic of rigid end (evident from bottom plots in Figure 3). The effect of conductivity shows that the free-end pattern is preserved up to a certain value of critical conductivity (shown as thick blue line in Figures 3b, and 3f), and the transformation of the mode is clearly seen beyond the upper limit of
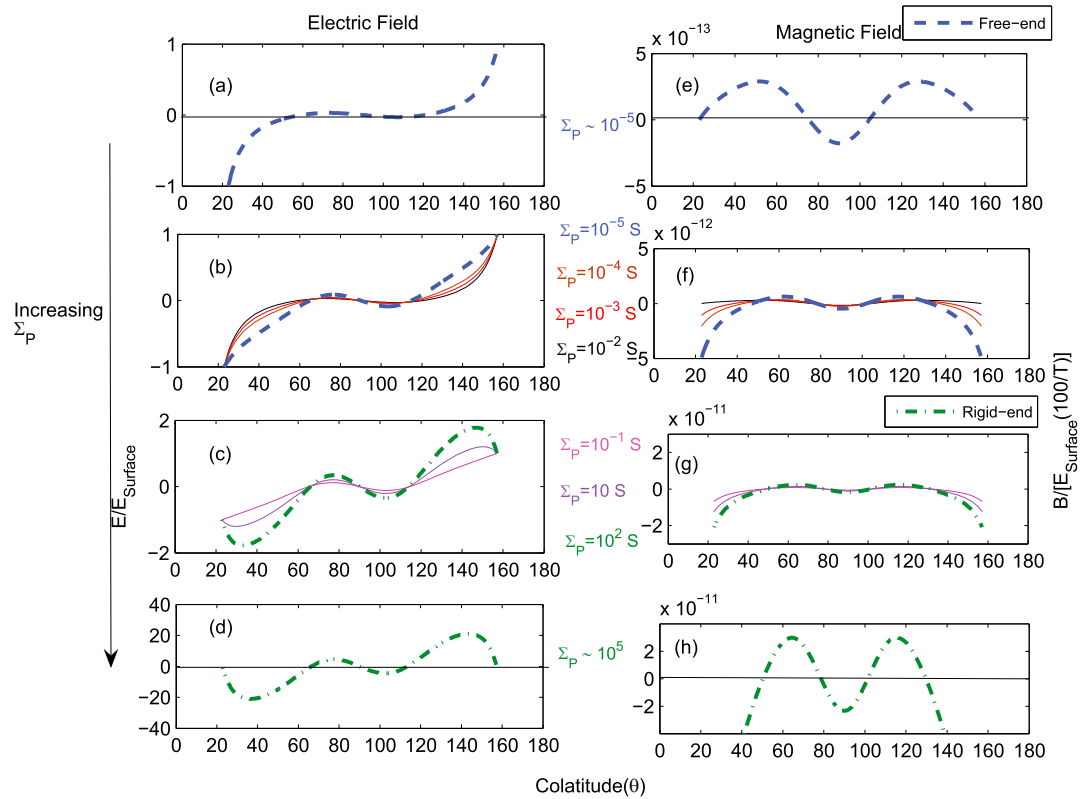
**Figure 3.** Same as for Figure 1 but for third harmonic.

critical conductivity (Figures 3c and 3g). The patterns of electric field and magnetic field shown in Figures 3d and 3h replicate the fourth harmonic rigid end, when the ionospheric conductivity is $\sim10^5$ S.

It is important to note that the symmetry is preserved at the equator during the mode transformation from free end to rigid end and vice versa. It is because of this symmetry that a change in the harmonic of the free end or rigid end is realized and is reflected in the spatiotemporal characteristics of the electric and magnetic field perturbations associated with the toroidal oscillations.

Similar exercise has been carried out to examine the effect of decreasing ionospheric conductivity (not shown here) on the toroidal oscillations. It is seen that a decrease in Σ_P from a significantly large value to a vanishingly small value connects a rigid-end mode to a free-end mode with a decrease in harmonic number by one. It is found that the fundamental rigid-end electric field does not have any counterpart in the free end [Figure 4]. The thick line in Figure 4a denotes the electric field structure for fundamental rigid end at $L = 6.6$ and for a typical density index $m = 5$. As the conductivity is decreased, the field line structure of the electric field shows a departure from the fundamental rigid end (shown as dotted lines in Figure 4a). The departure is maximum near the conjugate points and minimum at the equator. This implies that the effect of conductivity is maximum near the conjugate points in comparison to that at the equator. The corresponding DAM frequency obtained is 0.1044 cycles/s when the ionospheric conductivity is very large, $\sim10^5$ S (Figure 4b). With gradual decrement in conductivity, it is seen that the electric field structure gets modified and for sufficiently small value of conductivity (~10 S), the frequency estimated is 0.007 cycles/s which does not correspond to any harmonic of free end. This implies that the rigid-end fundamental does not have any counterpart in the free end. These features are consistent with the earlier numerical results by *Newton et al.* [1978] and *Yoshikawa et al.* [1999].

Although the mode and frequency conversions show consistent behavior with earlier workers, the results should be interpreted only in limits where $\gamma/\omega_r \ll 1$, i.e., for conductivities far from critical conductivity regimes where damping is insignificant. The limit of critical conductivity regime is decided by the balance of ionospheric Pedersen conductance Σ_P and the conductance of Alfvén wave Σ_A ($\Sigma_A = 1/\mu_0 V_A$) at the ionosphere.
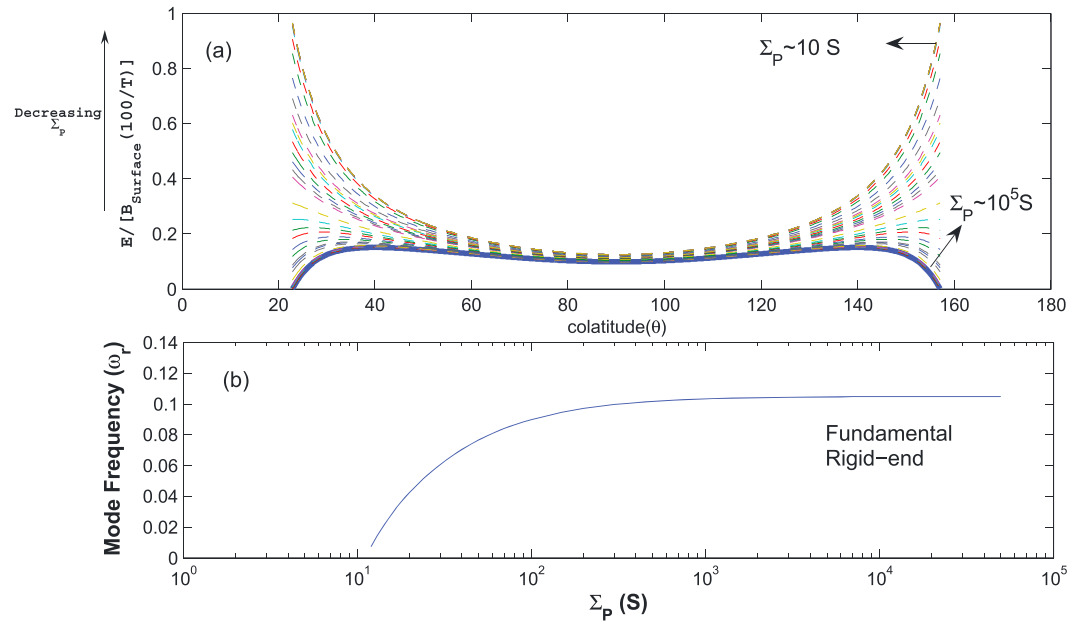
Figure 4. (a) Latitudinal structures of fundamental electric field of rigid end for decreasing Σ_P for $m = 5$ at $L = 6.6$. (b) Frequency characteristics of rigid-end fundamental with gradual decrease in Σ_P. $B_{surface}$ and T, respectively, represent the magnetic field at the conjugate point and wave period.

4. Nature of Standing Alfvén Waves in the Vicinity of $R = 0$ ($\Sigma_P \sim \Sigma_A$)

In this section, we discuss the nature of Alfvén waves when ionospheric damping is significant. *Bulusu et al.* [2015a] have made observations of oscillations where the mode frequency is affected with the change in the ionospheric conductivity. Although they addressed the mode-frequency change with respect to the ionospheric conductivity, they could not estimate the damping rate during this transformation. The studies by *Budnik et al.* [1998], *Obana et al.* [2008], and *Waters and Sciffer* [2008] also address such observations of mode transformations without throwing any light on the damping rate. In the following subsections we compute both mode frequency and the damping rate for different values of density index.

4.1. For Density Index $m = 6$

In the limit $R = 0$, the Pedersen conductance Σ_P is close to Σ_A. For these values of conductivity, damping is maximum and the standing mode is not possible. The dependence of mode frequency (ω_r) and damping (γ) on Σ_P is investigated using our developed analytic model for a particular density variation of $1/r^6$ (i.e., $m = 6$) along the field line. It should be noted that for such a density variation, the order of Bessel function will be $\nu = \pm 1/2$ ($\nu = 1/(r+2), r = 6 - m$), and the solution in equation (2) can be written as

$$X = \sqrt{\frac{2}{\pi \Omega L^2}} \left[\sin \Omega L (1 - \cos \theta) + K \cos \Omega L (1 - \cos \theta) \right] \qquad (8)$$

where $\Omega = \frac{\omega R_E}{V_{Aeq}}$ is the normalized frequency. Applying the boundary condition from equation (6) at the northern conjugate point and solving further we get

$$\left[\cos \Omega L (1 - \cos \theta_C) - K \sin \Omega L (1 - \cos \theta_c) \right] = i \mu_0 \Sigma_P V_{Aeq} \sqrt{1 + \cos^2 \theta_c} \left[\sin \Omega L (1 - \cos \theta_c) \right. $$
$$\left. + K \cos \Omega L (1 - \cos \theta_c) \right] \qquad (9)$$

It should be noted that the normalized frequency Ω is complex and can be given by $\Omega = \Omega_r + i\Gamma$, where $\Omega_r = \frac{R_E}{V_{Aeq}} \omega_r$ and $\Gamma = \frac{R_E}{V_{Aeq}} \gamma$ are, respectively, real and imaginary parts of normalized frequency Ω. Substituting this value of Ω in equation (9) and simplifying further we get

$$[\cos A \cosh B - i \sin A \sinh B] - K [\sin A \cosh B + i \cos A \sinh B]$$
$$- i \left(\frac{\Sigma_P}{\Sigma_A} \right) [[\sin A \cosh B + i \cos A \sinh B] + K [\cos A \cosh B + i \sin A \sinh B]] = 0 \qquad (10)$$

where $A = \Omega_r L(1 - \cos(\theta))$ and $B = \Gamma L(1 - \cos(\theta))$, and $\Sigma_A = \frac{1}{\mu_0 V_{Aeq}\sqrt{1+3\cos^2\theta_c}}$, which denotes Alfvén wave conductance at the conjugate point. The arbitrary constant K is evaluated by making either the solution X or its derivative dX/dS zero at the equator ($\theta = \pi/2$), depending on the harmonic number. The condition $X = 0$ at the equator relates to odd (even) harmonic of free end (rigid end), and the condition $\frac{dX}{dS} = 0$ corresponds to even (odd) harmonic of free end (rigid end), respectively. The condition $X = 0$ at the equator results in

$$K = -\frac{\tan\Omega_r L + i\tanh\Gamma L}{1 - i\tan\Omega_r L \tanh\Gamma L} \tag{11}$$

Substituting equation (11) in equation (10) and separating the real and imaginary parts we get the following two equations:

$$\cos(A - \Omega_r L)\left[\cosh(B - \Gamma L) + \frac{\Sigma_P}{\Sigma_A}\sinh(B - \Gamma L)\right] = 0 \tag{12}$$

and

$$\sin(A - \Omega_r L)\left[\sinh(B - \Gamma L) - \frac{\Sigma_P}{\Sigma_A}\cosh(B - \Gamma L)\right] = 0 \tag{13}$$

From equation (12) and equation (13) either $\cos(A - \Omega_r L) = 0$ or $\sin(A - \Omega_r L) = 0$.

The normalized mode frequency can thus be given by

$$\Omega_r = \frac{(2n + 1)\pi/2}{L\cos\theta_c} \tag{14}$$

$$\omega_r = \frac{V_{Aeq}}{R_E}\frac{(2n + 1)\pi/2}{L\cos\theta_c} \tag{15}$$

for asymmetric mode (quarter wave) and n varies as $n = 0, 1, 2, 3,...$ signifies different harmonics.

For symmetric half wave

$$\Omega_r = \frac{n\pi}{L\cos\theta_c} \tag{16}$$

$$\omega_r = \frac{V_{Aeq}}{R_E}\frac{n\pi}{L\cos\theta_c} \tag{17}$$

($n = 1, 2, 3,...$ denote different harmonics). It is important to note that the mode frequency is independent of Σ_P for $1/r^6$-type density variation.

An estimate of associated damping can be estimated by considering $\left[\cosh(B - \Gamma L) + \frac{\Sigma_P}{\Sigma_A}\sinh(B - \Gamma L)\right] = 0$ in equation (12) or $\left[\sinh(B - \Gamma L) - \frac{\Sigma_P}{\Sigma_A}\cosh(B - \Gamma L)\right] = 0$ in equation (13). Thus, normalized Γ can be expressed as

$$\Gamma = \frac{1}{L\cos\theta_c}\tanh^{-1}\left[\frac{\Sigma_A}{\Sigma_P}\right] \tag{18}$$

i.e.,

$$\gamma = \frac{V_{Aeq}}{R_E L\cos\theta_c}\tanh^{-1}\left[\frac{\Sigma_A}{\Sigma_P}\right] = \frac{V_{Aeq}}{R_E L\cos\theta_c}\ln\left|\frac{\Sigma_P + \Sigma_A}{\Sigma_P - \Sigma_A}\right| \tag{19}$$

The estimates of mode frequency ω_r and damping γ in equations (17) and (19) are consistent with earlier references [*Allan and Knox*, 1979a; *Southwood and Kivelson*, 2001].

Figure 5 denotes the variation of mode frequency and damping for a density variation of $1/r^6$ along the field line. It is clearly evident that the mode frequency ω_r is independent of conductivity for this particular density variation. This can be explained as follows. The Alfvén speed varies as $\frac{B}{\sqrt{\rho}}$, where B varies as $1/r^3$ and density ρ varies as $1/r^m$ along the field line. For a density index $m=6$, the decrease in the magnetic field is balanced by the change in the square root of density ($\sqrt{\rho}$) along the field line. Thus, the Alfvén speed is uniform (equal to the equatorial speed V_{Aeq}) all along the field line. This results in constant mode frequency independent of conductivity (cf. red line in Figure 5). In addition, it is seen that the damping is less in regions where $\Sigma_P \ll \Sigma_A$ or $\Sigma_P \gg \Sigma_A$. However, in the vicinity $\Sigma_P = \Sigma_A$, the damping is significantly large and standing structure is not possible.
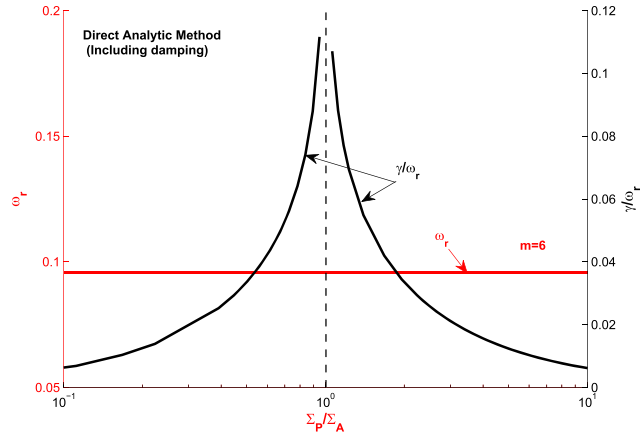
Figure 5. Variation of mode frequency (ω_r) and damping (γ/ω_r) with conductivity ratio Σ_P/Σ_A.

4.2. For Density Index $m \neq 6$

Different regions in the magnetosphere are characterized by different density variations along the field line [*Carpenter and Smith*, 1964; *Newbury et al.*, 1989; *Gallagher et al.*, 2000; *Goldstein et al.*, 2001; *Bulusu et al.*, 2015b]. In the preceding subsection, we discussed the effect of finite conductivity only for a particular field line density variation $1/r^6$. In this section, we extend our analysis to density variation other than $1/r^6$ ($m = 6$) type. There have been numerical studies in the past that addressed the effect of ionospheric conductivity on toroidal oscillations [*Newton et al.*, 1978; *Yoshikawa et al.*, 1999]. They first time numerically modeled the mode transformation with ionospheric conductivity in different magnetic field geometries. The analytic studies undertaken could not address this because they were based on a typical density profile of $1/r^6$ along the field line [*Allan and Knox*, 1979a; *Ozeke and Mann*, 2005]. This particular density variation does not address the general scenario as density variation obeys different power law in different regions of the magnetosphere [*Carpenter and Smith*, 1964; *Newbury et al.*, 1989; *Gallagher et al.*, 2000; *Goldstein et al.*, 2001].

In order to address this, we rewrite the solution for the domain $\eta > \nu$. In this limit, Bessel function in equation (2) can be expanded asymptotically as

$$J_\nu(\eta) = \sqrt{\frac{2}{\pi\eta}} \cos\left(\eta - \frac{\pi}{2}\nu - \frac{\pi}{4}\right) \tag{20}$$

and

$$J_{-\nu}(\eta) = \sqrt{\frac{2}{\pi\eta}} \cos\left(\eta + \frac{\pi}{2}\nu - \frac{\pi}{4}\right) \tag{21}$$

It should be noted that the term η is given as $\eta = \Omega L \int_0^\theta \sin^{7-m}\theta$ for the Northern Hemisphere, and $\eta = \Omega L \int_\theta^\pi \sin^{7-m}\theta$ for the Southern Hemisphere. In order to account for damping, Ω is made complex as discussed in the earlier section resulting into the following equation using the appropriate boundary conditions at the conjugate ionospheres.

$$(3 - m/2)\cot(\theta_c)\left[\cos\alpha\cosh\beta - i\sin\alpha\sinh\beta\right] + (\Omega_r + i\Gamma)L\sin^{(7-m)}\theta_c\left[\sin\alpha\cosh\beta + i\cos\alpha\sinh\beta\right]$$

$$- iL(\Omega_r + i\Gamma)\sin^{6-m}\theta_c\left(\frac{\Sigma_P}{\Sigma_A}\right)\left[\cos\alpha\cosh\beta - i\sin\alpha\sinh\beta\right] = 0 \tag{22}$$

where $\alpha = \Omega_r L\left[\int_0^{\theta_c}\sin^{7-m}\theta - \int_0^{\pi/2}\sin^{7-m}\theta\right]$ and $\beta = \Gamma L\left[\int_0^{\theta_c}\sin^{7-m}\theta - \int_0^{\pi/2}\sin^{7-m}\theta\right]$.

The behavior of mode frequency and damping coefficient with respect to ionospheric conductivity at the conjugate points has been examined using the perturbation technique around the standard density index $m = 6$,
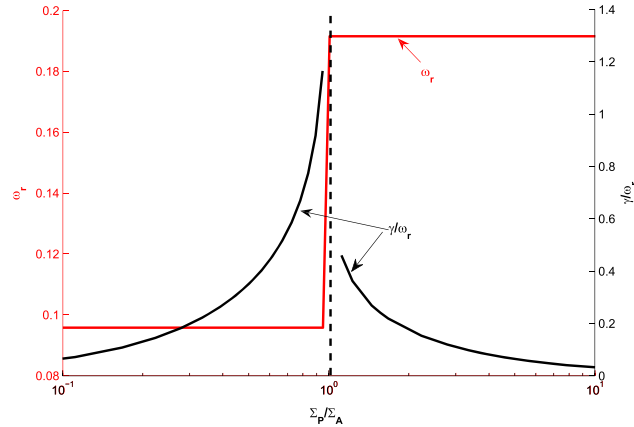
Figure 6. Variation of mode frequency (ω_r) and damping (γ/ω_r) with conductivity ratio Σ_P/Σ_A for a perturbation of 0.1.

where their behavior is well known as discussed in section 4.1. Considering perturbation only up to the first order, equation (22) can be written as

$$T1_{m=6} + m1\left(\frac{\mathrm{d}}{\mathrm{d}m}(T1)\right)_{m=6} + T2_{m=6} + m1\left(\frac{\mathrm{d}}{\mathrm{d}m}(T2)\right)_{m=6} + T3_{m=6} + m1\left(\frac{\mathrm{d}}{\mathrm{d}m}(T3)\right)_{m=6} = 0 \qquad (23)$$

where, $T1$, $T2$, and $T3$ denote, respectively, the first, second, and third terms of equation (22), $m1$ denotes the first-order perturbation ($m1 \ll 6$), and the suffix $m = 6$ denotes the value of the parameter at $m = 6$. Solving equation (22) using the perturbation technique in equation (23) we get,

$$\frac{m1}{2L(\Omega_r + i\Gamma)}\frac{\cot\theta_c}{\sin\theta_c}\cos(\alpha_{m6} + i\beta_{m6}) + \left[(1 + m1\ln\sin\theta_c)\sin(\alpha_{m6} + i\beta_{m6}) + m1L(\Omega_r + i\Gamma)R\cos(\alpha_{m6} + i\beta_{m6})\right]$$

$$- iL(\Omega_r + i\Gamma)\sin^{6-m}\theta_c\left(\frac{\Sigma_P}{\Sigma_A}\right)\left[\cos(\alpha_{m6} + i\beta_{m6}) + m1RL(\Omega_r + i\Gamma)\sin(\alpha_{m6} + i\beta_{m6})\right] = 0 \qquad (24)$$

where α_{m6} and β_{m6} represent, respectively, the values of α and β at $m = 6$. The above equation is decoupled to real and imaginary parts in order to form two simultaneous equations.

Further, the normalized mode frequency is expressed as $\Omega_r = \Omega_0 + \Omega_1$, where Ω_0 is the mode frequency at $m = 6$ and Ω_1 is the first-order correction to Ω_0. In the similar manner, damping factor Γ is expressed as $\Gamma = \Gamma_0 + \Gamma_1$, where Γ_0 denotes the damping corresponding to $m = 6$ and Γ_1 is the first-order correction to damping. Substituting the expression of Ω_r and Γ in equation (24) and solving we get two simultaneous equations as

$$\Omega_1 f_1 + \Gamma_1 g_1 = -k_1 m1 - \Omega_1 f_2 + \Gamma_1 g_2 = -k_2 m1 \qquad (25)$$

where f_1, g_1, f_2, and g_2 are functions of $(\Omega_0, \Gamma_0, \Sigma_P/\Sigma_A)$. k_1 and k_2 are functions of (Ω_0, Γ_0). Equation (25) can be solved for Ω_1 and Γ_1 using Cramer's rule.

It is evident that for a typical density profile of $1/r^6$ along the field line, the mode frequency is independent of ionospheric conductivity [*Newton et al.*, 1978; *Allan and Knox*, 1979a; *Yoshikawa et al.*, 1999]. This is reported in the present study as well (in subsection 4.1). However, for slight deviation from this density variation, the mode frequency would show a dependency on ionospheric conductivity. This can be explained on physical grounds. For density indices other than $m = 6$, the density variation $\left(\sqrt{\rho}\right)$ is less steep compared to the variation of magnetic field strength along a field line. This leads to an increased Alfvén speed as we move away from the equator along the field line. In order to account for this dependency, we have used the perturbation technique. In the next section, we discuss case studies presenting the results from perturbation techniques.

4.3. Case Studies of Perturbation Technique
4.3.1. Perturbation, $m1$=0.1
For a perturbation of 0.1 around density index $m = 6$, the variation of ω_r and γ/ω_r is shown in Figure 6. A striking thing to note here is that with slight deviation of 0.1 (i.e., ~1.5%) from $m = 6$, the mode frequency (ω_r)
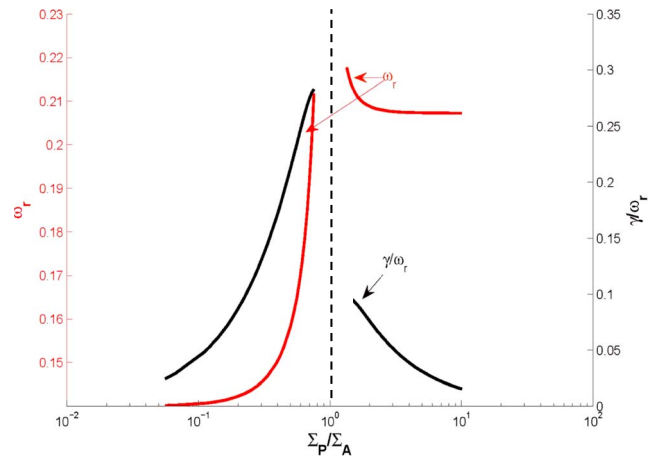
Figure 7. Variation of mode frequency (ω_r) and damping (γ/ω_r) with conductivity ratio Σ_P/Σ_A for a perturbation of 0.5.

shows a clear dependence on conductivity (Σ_P/Σ_A). Away from the critical regime ($\Sigma_P \simeq \Sigma_A$), the mode frequency does not show any significant variation. However, as Σ_P approaches Σ_A, mode frequency (ω_r) increases significantly (almost twice). A consistent feature of increased damping in the vicinity of $\Sigma_P = \Sigma_A$ is realized in this case also [cf. Figure 6].

4.3.2. Perturbation, $m1=0.5$

Variation of ω_r and γ/ω_r with conductivity ratio for a perturbation of 0.5 ($\sim$3%) around density index $m = 6$, are shown in Figure 7. The variation of mode frequency (ω_r) is pronounced in the vicinity of Alfvén conductance Σ_A. In addition, the width of the damping region also increases with increase in perturbation apart from showing a jump around $\Sigma_P \sim \Sigma_A$.

4.3.3. Perturbation, $m1=1$

For a perturbation of $m1 = 1$ around $m = 6$, the mode transformation is clearly seen from Figure 8. It should be noted that both ω_r and γ/ω_r show singular behavior around $\Sigma_P \sim \Sigma_A$. The fundamental mode frequency corresponding to free end ($\frac{\Sigma_P}{\Sigma_A} \ll 1$) is around 0.19 cycles/s (departure of $\sim$30% from numerically computed mode frequency [*Bulusu et al.*, 2015b]). However, as Σ_P is increased, the rigid-end second harmonic is realized and the percentage departure of mode frequency becomes less than 5% from the value computed using numerical methods [*Bulusu et al.*, 2015b]. The variation of γ/ω_r is increasingly asymmetric around $\Sigma_P \sim \Sigma_A$ when compared to the earlier cases (Figures 7 and 6).
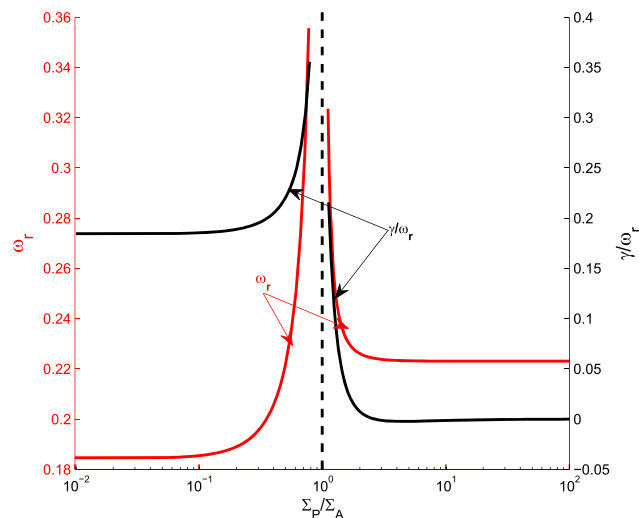
Figure 8. Variation of mode frequency (ω_r) and damping (γ/ω_r) with conductivity ratio Σ_P/Σ_A for a perturbation of 1.0.

Thus, it can be seen that as we depart from density index $m = 6$, the effect of conductivity on mode frequency and damping increases. This can be explained as follows. For density indices other than $m = 6$, the density variation $\left(\sqrt{\rho}\right)$ is less steep compared to the variation of magnetic field strength along a field line. This leads to an increased Alfvén speed as we move away from equator along the field line, thereby affecting the change in the associated Alfvén wave conductance which in turn changes the mode frequency and period of the wave.

5. Conclusions

In this paper, we addressed the effect of finite ionospheric conductivities on field line, using analytic model. It was seen from the developed analytic model that when the ionospheric conductivity was gradually increased for a particular mode from a small value to a large value, the characteristic free-end mode gets transformed to a rigid-end mode with an increase in harmonic number by one and vice versa. This result is not new but is still an improvement over the earlier work because the earlier analytic results were obtained only for a particular value of density ($m = 6$) which corresponds to simple harmonic equation [*Allan and Knox*, 1979a]. Moreover, it was seen that the regime of conductivities within which the frequency changed drastically for a small change in conductivity (called critical conductivity) decreased with increase in mode number. In the lower limits of $\frac{\Sigma_P}{\Sigma_A} \ll 1$, the mode frequency resembles a free end which transforms to subsequent higher harmonic of rigid end in the limit $\frac{\Sigma_P}{\Sigma_A} \gg 1$. However, the rigid-end fundamental does not have any counterpart in the free-end domain. Although in the present study we have presented result for L shell 6.6, the study is applicable for all L shells beyond $L = 2$ onward till the validity of dipole approximation.

One important issue that needs to be addressed is the damping rate of the wave at the ionosphere due to finite conductivity. The expression for damping has been developed for the simple harmonic case ($m = 6$) which matches with the earlier results [*Allan and Knox*, 1979a; *Southwood and Kivelson*, 2001]. Here we compute the damping effect for density index other than the standard $m = 6$ index, using perturbation technique. It is seen that for a density variation of $1/r^6$ type, the mode frequency ω_r is independent of Σ_P. However, with slight change in the density index, the mode frequency showed a dependence on ionospheric conductance Σ_P. The corresponding rate of damping γ/ω_r shows a sharp increase in the vicinity of $\Sigma_P \sim \Sigma_A$, and standing wave structure is not possible for $\Sigma_P = \Sigma_A$ (i.e., $R = 0$). In fact, it is in this region where the mode transformation is affected. The damping width increases with increasing departure of density index m from $m = 6$. It is interesting to note that even from our computation we obtain the damping rates to be of the order of 0.14–0.2 (which is close to earlier results [*Newton et al.*, 1978]). Away from the critical conductivity regime, the damping is negligible. In this study, we have addressed only the damping rate for $m = 5$–6. A generalized analytic expression of damping rate that can be applied to any density variation still remains an open question. This can be achieved by solving equation (24) in the complex frequency domain, which forms a part of our future study.

Appendix A: Assumptions and Complete Derivation of Equation (1)

Mode equation (1) describes the low-frequency waves in infinitely conducting, stationary, magnetized plasma with zero pressure. This equation was derived by using basic MHD equations to estimate the period and amplitude of low-frequency transverse waves in an arbitrary field geometry.

Faraday's law

$$\vec{\nabla} \times \vec{E} = \frac{\partial \vec{b}}{\partial t} \tag{A1}$$

Ohm's law under infinite conductivity (or frozen-in-flux condition) can be given by

$$\vec{E} = -\frac{\partial \vec{\xi}}{\partial t} \times \vec{B_0} \tag{A2}$$

Ampere's law

$$\vec{\nabla} \times \vec{b} = \mu_0 \vec{j} \tag{A3}$$

Momentum equation

$$\rho \frac{\partial^2 \vec{\xi}}{\partial t^2} = \vec{j} \times \vec{B_0} \tag{A4}$$

where $\vec{B_0}$ is the unperturbed magnetic field, $\vec{E}$ and $\vec{b}$ are perturbed electric and magnetic field associated with the Alfvén wave. $\vec{\xi}$ is the displacement of plasma (or field), $\vec{j}$ is the associated current, and ρ is the plasma mass density.

The wave equation satisfied by the field displacement $\vec{\xi}$ can be obtained as

$$\left[\partial^2 \left(\vec{B_0} \times \vec{\xi} \right) / \partial t^2 \right] = \vec{V_A} \times \vec{V_A} \times \left(\vec{\nabla} \times \vec{\nabla} \times \left(\vec{B_0} \times \vec{\xi} \right) \right) \tag{A5}$$

where $\vec{V_A} = \frac{\vec{B_0}}{\sqrt{\mu_0 \rho}}$ is the Alfvén speed associated with the wave. This equation is the starting point for obtaining the solution for long-period geomagnetic field line oscillations. Numerous authors have solved this equation numerically in different ambient field geometries [*Dungey*, 1963; *Radoski*, 1967; *Cummings et al.*, 1969; *Orr and Mathew*, 1971]. *Singer et al.* [1981] developed a generalized mode equation to address the toroidal and poloidal oscillations.

In order to examine the oscillation of isolated field lines two adjacent field lines were assumed to be separated at some point along the normal by distance δ_α. At any other point along the field line, the normal separation can be obtained by multiplying with the scale factor h_α as $h_\alpha \delta_\alpha$. The normal unit vector $\hat{\alpha}$ between the field lines can be written as $\vec{\nabla}\alpha = \hat{\alpha}/h_\alpha$.

The magnetic field perturbations b associated with a small displacement ξ_α can be obtained from equations (A1) and (A2) as

$$\vec{b} = \vec{\nabla} \times \left(\xi_\alpha \hat{\alpha} \times \vec{B_0} \right) \tag{A6}$$

It can be seen that

$$\vec{b} \cdot \vec{\nabla}\alpha = \vec{\nabla}\alpha \cdot \vec{\nabla} \times \left(\xi_\alpha h_\alpha \vec{\nabla}\alpha \times \vec{B_0} \right) = \vec{\nabla} \cdot \left(\xi_\alpha h_\alpha |\nabla\alpha|^2 \times \vec{B_0} \right)$$

Since $\nabla\alpha$ is perpendicular to B_0, it is evident that $|\nabla\alpha|^2 = 1/h_\alpha^2$ and thus,

$$\vec{b} \cdot \vec{\nabla}\alpha = (b_\alpha/h_\alpha) = \vec{B_0} \cdot \vec{\nabla} \times (\xi_\alpha/h_\alpha) \tag{A7}$$

The magnetic perturbation b_α, using equations (A3) and (A4), produces a force in the momentum equation as

$$\mu_o \rho \frac{\partial^2 \xi_\alpha}{\partial t^2} = \left(\frac{1}{h_\alpha} \right) \left(\vec{B_0} \cdot \vec{\nabla} b_\alpha h_\alpha \right) \tag{A8}$$

Equations (A8) and (A7) can be rearranged to give the wave equation as equation (1). Once ξ_α is known the spatial structure for electric and magnetic field can be obtained using

$$b_\alpha = h_\alpha B_o \frac{\mathrm{d}}{\mathrm{d}S} \left(\frac{\xi_\alpha}{h_\alpha} \right) \tag{A9}$$

$$E_\beta = -i\omega \xi_\alpha B_o \tag{A10}$$

where $(B_0/B, \alpha, \beta)$ form a right-handed orthogonal system. The versatility of the above equation is seen from its applicability to both dipolar and nondipolar magnetic field geometry, and this equation can be solved for uncoupled toroidal and poloidal oscillations in general. This equation has been used by numerous authors for obtaining both the field line structures and plasma density estimates.

Appendix B: Assumptions and Complete Derivation of Equation (2)

Previous analytic attempt involves computation of time of flight of ULF waves between the conjugate points using WKB method [*Warner and Orr*, 1979]. However, *Singer et al.* [1981] stated that WKB approximation is not valid when the wavelength of the oscillation is comparable to the scale size of the system and is particularly poor for the fundamental mode oscillation of a field line. If the argument was true then for higher harmonics, especially third harmonic onward, the departure in WKB frequency from the numerical exact frequency should be negligibly small. *Sinha and Rajaram* [1997] showed that the departure in the frequency got saturated with

increasing harmonic number and did not vanish even for the harmonic as large as 20. They attributed this discrepancy to the inability of the method in handling the singularities at the turning points (colatitude $\theta \sim 0$ and $\theta \sim \pi$). They could obtain a natural and self-consistent analytic solution for the toroidal eigenmodes in the dipole field geometry by ensuring that the solution was well behaved throughout. Below we briefly outline the solution obtained by *Sinha and Rajaram* [1997] which has been used in the present study.

Sinha and Rajaram [1997] solved equation (1) using both analytic and numerical methods using the following assumptions.

1. The background magnetic field is dipolar.
2. Perturbed quantities vary as $\exp[i\omega\tau]$.
3. Density variation is governed by the power law $\rho = \rho_o(r_o/r)^m$, where m is the density index and ρ_o is proton mass density at r_o, the geocentric distance to equatorial crossing point of the field line considered, and r is the geocentric distance to the position of interest on the field line.
4. The field lines are rigidly fixed at their ends in the ionosphere (ionosphere is infinitely conducting).

Equation (1) was made dimensionless by making the following normalization.

$$S = \frac{s}{R_E}, \Omega = \frac{\omega R_E}{V_{Aeq}}, X = \frac{\xi_\alpha}{R_E h_\alpha}, B = \frac{B_o}{B_{eq}} \tag{B1}$$

where s is the distance measured along the ambient magnetic field line from the equatorial plane. R_E is the Earth's radius, V_{Aeq} is the Alfvén velocity at the equator, B_{eq} is the ambient magnetic field at the equator, and θ is the colatitude.

The dimensionless form of equation (1) is given by

$$-\frac{\Omega^2}{\sin^{2m}\theta}X = \frac{B}{h_\alpha^2}\frac{d}{dS}\left[h_\alpha^2 B\frac{dX}{dS}\right] \tag{B2}$$

With the assumption that the background magnetic field is dipolar, the parameters h_α, B, and B_{eq} are given by the following expressions. $h_\alpha = L\sin^3\theta$ for the toroidal mode, $B = \sqrt{1 + 3\cos^3\theta}/\sin^6\theta$, and $B_{eq} = 0.311/L^3$ Gauss. The suffix c indicates the value at the conjugate point, and $L = 1/\sin^2\theta_c$ is the geocentric distance (in Earth radius) of the point where the field line crosses the equator.

Equation (B2) can be transformed to standard WKB form [*Bender and Orszag*, 1978]

$$\epsilon^2\frac{d^2X}{dv^2} + \Phi(v)X = 0 \tag{B3}$$

where

$$\frac{dv}{dS} = \frac{1}{h_\alpha^2 B}, \epsilon = 1/L^2, \Phi(v) = \Omega^2\sin^{12-2m}\theta, \ h_\alpha = L\sin^3\theta \tag{B4}$$

for the toroidal mode.

The WKB solutions can be obtained by considering the eigenfunction to vanish (infinitely conducting ionosphere) at the ionosphere. However, the solutions thus obtained using standard WKB method failed terribly for the fundamental, especially near the conjugate points. The failure was attributed to the scale size of the variation which was of the order of the scale size of the system for the fundamental. This is due to the inability of the formal WKB method to address the singularity at the turning points ($\theta \sim 0$ or $\theta \sim \pi$ in equation (B3)). They suggested an improvement based on the *Langer* [1994] approach which ensures the continuity of the solutions at the turning points. According to this approach, the singular function $\Phi(v)$ can be expressed as a product of two functions v^r, where r is a number and $\Psi(v)$, where all the singularities are imparted to the factor v^r and $\Psi(v) = \Phi(v)/v^r$ remains well behaved throughout including the turning points.

This leads to

$$\epsilon^2\frac{d^2X}{dv^2} + v^r\Psi(v)X = 0 \tag{B5}$$

By making the transformations $X = a(v)Z, a(v) \neq 0, \zeta = \zeta(v), a(v) = (d\zeta/dv)^{-1/2}$, and $\zeta^r(d\zeta/dv)^2 = v^r\Psi(v)$, equation (B5) takes the form

$$\left[\frac{d^2}{d\zeta^2} + \frac{\zeta^r}{\epsilon^2} + a^3\frac{d^2a(v)}{dv^2}\right]Z = 0 \tag{B6}$$

On the basis of analytic and numerical grounds, the third term in equation (B6) is neglected (For justification refer to *Sinha and Rajaram* [1997] and *Bulusu et al.* [2015b]) and transformed to the following standard Bessel equation

$$\frac{d^2 u}{d\eta^2} + \frac{1}{\eta}\frac{du}{d\eta} + \left[1 - \frac{\nu^2}{\eta^2}\right]u = 0 \tag{B7}$$

where $\eta = (2/\epsilon)\zeta^{r+2/2}/(r+2)$, $Z = \sqrt{\zeta}u$, and $\nu = 1/(r+2)$, $(r = 6 - m)$. Equation (B7) was solved in two hemispheres, and it is ensured that the solution was analytically continuous by matching the solution and its derivative at the equator. It should be noted that $\eta = \frac{\omega L R_E}{V_{\text{Aeq}}}\int_0^\theta \sin^{7-m}\theta$ for the Northern Hemisphere, and $\eta = \frac{\omega L R_E}{V_{\text{Aeq}}}\int_\theta^\pi \sin^{7-m}\theta$ for the Southern Hemisphere. Finally, the solution of equation (B7) in terms of normalized displacement X can be written as equation (2).

The significance of this solution lies in its applicability to different ionospheric conditions [*Bulusu et al.*, 2014a, 2015a]. The associated electric and magnetic field can be obtained by slight rearrangements of equations (A9) and (A10) as

$$b = h_\alpha B_0 \frac{dX}{dS} \tag{B8}$$

and

$$E = -i\Omega V_{\text{Aeq}} h_\alpha B_0 \tag{B9}$$

References

Agapitov, A. V., O. K. Cheremnykh, and A. S. Parnowski (2008), Ballooning perturbations in the inner magnetosphere of the Earth: Spectrum, stability and eigenmode analysis, *Adv. Space Res.*, *41*, 1682–1687.

Allan, W., and F. B. Knox (1979a), A dipole field model for axisymmetric Alfvén wave with finite ionospheric conductivities, *Planet. Space Sci.*, *27*, 79–85.

Allan, W., and F. B. Knox (1979b), The effect of finite ionospheric conductivities on axisymmetric toroidal Alfvén wave resonances, *Planet. Space Sci.*, *27*, 939–950.

Anderson, B. J., M. J. Engebretson, S. P. Rounds, L. J. Zanetti, and T. A. Potemra (1990), A statistical study of Pc3-5 pulsations observed by the AMPTE/CCE magnetic fields experiment. 1. Occurrence distributions, *J. Geophys. Res.*, *95*, 10,495–10,523.

Baker, W. G., and D. F. Martyn (1953), Electric currents in the ionosphere. The conductivity, *Philos. Trans. R. Soc. A*, *246*, 281–294.

Bender, C. M., and S. A. Orszag (1978), *Advanced Mathematical Methods for Scientists and Engineers*, McGraw-Hill International Book Company, Springer, New York.

Bochev, A. Z., and A. K. Sinha (2010), A coordinated study of field-aligned currents and Pc5 ULF waves during ejecta 1997, *Adv. Space Res.*, *46*, 1111–1119.

Budnik, F., M. Stellmacher, K. H. Glassmeier, and S. C. Buchert (1998), Ionospheric conductance distribution and MHD wave structure: Observation and model, *Ann. Geophys.*, *16*(2), 140–147.

Bulusu, J., A. K. Sinha, and G. Vichare (2014a), Toroidal quarter waves in the Earth's magnetosphere: Theoretical studies, *Astrophys. Space Sci.*, *353*, 395–404, doi:10.1007/s10509-014-2052-2.

Bulusu, J., A. K. Sinha, and G. Vichare (2015a), Toroidal quarter waves in the Earth's magnetosphere: Observational perspective, *Astrophys. Space Sci.*, *357*, 13, doi:10.1007/s10509-015-2306-7.

Bulusu, J., A. K. Sinha, and G. Vichare (2015b), An analytic model of toroidal half-wave oscillations: Implication on plasma density estimates, *J. Geophys. Res. Space Physics*, *120*, 4164–4180, doi:10.1002/2014JA020797.

Carpenter, D. L., and R. L. Smith (1964), Whistler measurements of electron density in the magnetosphere, *Rev. Geophys.*, *71*, 415–441.

Cummings, W. D., R. J. O'Sullivan, and P. J. Coleman (1969), Standing Alfvén waves in the magnetosphere, *J.Geophy. Res.*, *74*, 778–793.

Denton, R. E., K. Takahashi, R. R. Anderson, and M. P. Wuest (2004), Magnetospheric toroidal Alfvén wave harmonics and the field line distribution of mass density, *J. Geophys. Res.*, *109*, A06202, doi:10.1029/2003JA010201.

Dungey, J. W. (1954), Electrodynamics of the outer atmospheres, *Rep. 69*, Ions. Res. Lab. Pa. State Univ.

Dungey, J. W. (1963), Hydromagnetic waves and the ionosphere, in *Proceedings International Conference on the Ionosphere*, pp. 230–232, Inst. of Physics, London.

Ellis, P., and D. J. Southwood (1983), Reflection of Alfvén waves by non-uniform ionospheres, *Planet. Space Sci.*, *31*, 107–117.

Engebretson, M. J., L. J. Zanetti, T. A. Potemraa, and M. H. Acufia (1986), Harmonically structured ULF pulsations observed by AMPTE/CCE magnetic field experiment, *Geophys. Res. Let.*, *13*, 905–908.

Gallagher, D. L., P. D. Craven, and R. H. Comfort (2000), Global core plasma model, *J. Geophys. Res.*, *105*, 18,819–18,33.

Goldstein, J., R. E. Denton, M. K. Hudson, E. G. Miftakhova, S. L. Young, J. Menietti, and D. Gallagher (2001), Latitudinal density dependence of magnetic field lines inferred from polar plasma wave data, *J. Geophys. Res.*, *106*, 6195–6201.

Hughes, W. J. (1974), The effect of the atmosphere and ionosphere on long period magnetospheric micropulsations, *Planet. Space Sci.*, *22*, 1157–1172.

Hughes, W. J., and D. J. Southwood (1976), The screening of micropulsation signals by the atmosphere and ionosphere, *J. Geophys. Res.*, *81*, 3234–3240.

Inoue, Y. (1973), Wave polarizations of geomagnetic pulsations observed in high latitudes on the Earth's surface, *J. Geophys. Res.*, *78*, 2959–2976.

Langer, R. E. (1994), The asymptotic solutions of ordinary linear differential equations of second order, with special reference to a turning point, *Trans. Am. Math. Soc.*, *67*, 461–490.

Liu, W., J. B. Cao, X. Li, T. E. Sarris, Q.-G. Zong, M. Hartinger, K. Takahashi, H. Zhang, Q. Q. Shi, and V. Angelopoulos (2013), Poloidal ULF wave observed in the plasmasphere boundary layer, *J. Geophys. Res. Space Physics*, *118*, 4298–4307, doi:10.1002/jgra.50427.

Lysak, R. L. (2004), Magnetosphere-ionosphere coupling by Alfvén waves at midlatitudes, *J. Geophys. Res*, *109*, A07201, doi:10.1029/2004JA010454.

Maltsev, Y. P., W. B. Lyatsky, and A. M. Lyatskaya (1977), Currents over an auroral arc, *Planet. Space Sci.*, *25*, 53–57.

McClay, J. F. (1970), On the resonant modes of a cavity and the dynamical properties of micropulsations, *Planet. Space Sci.*, *18*, 1673–1690.

Nakata, H., S. Fujita, A. Yoshikawa, M. Itonaga, and K. Yumoto (2000), Ground magnetic perturbations associated with the standing toroidal mode oscillations in the magnetosphere-ionosphere system, *Earth Planets Space*, *52*, 601–613.

Newbury, I. T., R. H. Comfort, P. G. Richard, and C. R. Chappell (1989), Thermal He$^+$ in the plasmasphere: Comparison of observations with numerical calculations, *J. Geophys. Res.*, *94*, 15,265–15,276.

Newton, R. S., D. J. Southwood, and W. J. Hughes (1978), Damping of geomagnetic pulsations by the ionosphere, *Planet. Space Sci.*, *26*, 201–209.

Nishida, A. (1964), Ionospheric screening effect and storm sudden commencement, *J. Geophys., Res.*, *69*, 1861–1874.

Obana, Y., F. W. Menk, M. D. Sciffer, and C. L. Waters (2008), Quarter-wave modes of standing Alfvén waves detected by cross-phase analysis, *J. Geophys. Res.*, *113*, A08203, doi:10.1029/2007JA012917.

Orr, D. (1973), Magnetic pulsations within the magnetosphere: A review, *J. Atmos. Terr. Phys.*, *35*, 1–51.

Orr, D., and J. A. D. Mathew (1971), The variation of geomagnetic micropulsation periods with latitude and the plasmapause, *Planet. Space Sci.*, *19*, 897–905.

Ozeke, L. G., and I. R. Mann (2005), High and low ionospheric conductivity standing guided Alfvén wave eigenfrequencies: A model for plasma density mapping, *J. Geophys. Res.*, *110*, A04215, doi:10.1029/2004JA010719.

Radoski, H. R. (1967), A note on oscillating field lines, *J. Geophys. Res.*, *72*, 418–419.

Scholer, M. (1970), On the motion of artificial ion clouds in the magnetosphere, *Planet. Space Sci.*, *18*, 977–1004.

Singer, H. J., D. J. Southwood, R. J. Walker, and M. G. Kivelson (1981), Alfvén wave resonances in a realistic magnetospheric magnetic field geometry, *J. Geophys. Res.*, *86*, 4589–4596.

Sinha, A. K., and R. Rajaram (1997), An analytic approach to toroidal eigen mode, *J. Geophys. Res.*, *102*, 17,649–17,657.

Sinha, A. K, T. K. Yeoman, J. A Wild, D. M. Wright, S. W. H. Cowley, and A. Balogh (2005), Evidence of transverse magnetospheric field line oscillations as observed from Cluster and ground magnetometers, *Ann. Geophys.*, *23*, 919–929.

Southwood, D. J. (1974), Some features of field line resonances in the magnetosphere, *Planet. Space Sci.*, *22*, 483–491.

Southwood, D. J., and M. G. Kivelson (2000), Relationships between structure and energy flux in magnetohydrodynamic waves in magnetosphere, *J. Geophys. Res.*, *105*, 27,701–27,706.

Southwood, D. J., and M. G. Kivelson (2001), Damping standing Alfvén waves in the magnetosphere, *J. Geophys. Res.*, *106*, 10,829–10,836.

Streltsov, A., and W. Lotko (1996), The fine structure of dispersive, nonradiative field line resonance layers, *J. Geophys. Res.*, *101*, 5343–5358.

Takahashi, K., and R. E. Denton (2007), Magnetospheric seismology using multiharmonic toroidal waves observed at geosynchronous orbit, *J. Geophys. Res.*, *112*, A05204, doi:10.1029/2006JA011709.

Takahashi, K., M. D. Hartinger, V. Angelopoulos, K.-H. Glassmeier, and H. J. Singer (2013), Multispacecraft observations of fundamental poloidal waves without ground magnetic signatures, *J. Geophys. Res. Space Physics*, *118*, 4319–4334, doi:10.1002/jgra.50405.

Tamao, T. (1964), The structure of three-dimensional hydromagnetic waves in a uniform cold plasma, *J. Geomagn. Geoelectr.*, *16*, 89–114.

Tu, J., P. Song, and V. M. Vasyliūnas (2014), Inductive-dynamic magnetosphere-ionosphere coupling via MHD waves, *J. Geophys. Res. Space Physics*, *119*, 530–547, doi:10.1002/2013JA018982.

Warner, M. R., and D. Orr (1979), Time of flight calculations for high latitude geomagnetic pulsations, *Planet. Space Sci.*, *27*, 679–689.

Waters, C. L., and M. D. Sciffer (2008), Field line resonant frequencies and ionospheric conductance: Results from a 2-D MHD model, *J. Geophys. Res.*, *113*, A05219, doi:10.1029/2007JA012822.

Yagova, N., V. Pilipenko, E. Fedorov, M. Vellante, and K. Yumoto (1999), Influence of ionospheric conductivity on midlatitude Pc3-4 pulsations, *Earth Planets Space*, *51*, 129–138.

Yoshikawa, A., and M. Itonaga (1996), Reflection of shear Alfvén waves at the ionosphere and the divergent Hall current, *Geophys. Res. Let.*, *23*, 101–104.

Yoshikawa, A., M. Itonaga, S. Fujita, H. Nakata, and K. Yumoto (1999), Eigen mode analysis of field line oscillations interacting with the ionosphere atmosphere-solid Earth electromagnetic coupled system, *J. Geophys. Res.*, *104*, 28,437–28,457.